Models of Secondary Nucleation Attributable to Crystal-Crystallizer and Crystal-Crystal Collisions

The rate of secondary nucleation of ice, assumed to be proportional to the product of collision frequency and impact energy, has been quantitatively modeled using idealized representations of collisions between crystals and either other crystals or surfaces in the crystallizer. The crystal-crystallizer collisions were assumed to be driven by either steady or turbulent fluid motion and the crystal-crystal collisions were assumed to be driven by either gravitational forces or turbulent eddies. The models predict to a good approximation the experimentally determined dependence of the secondary nucleation of ice on crystal size, ice concentration, and agitation power.

T. W. EVANS
A. F. SAROFIM
and
G. MARGOLIS

Department of Chemical Engineering
Massachusetts Institute of Technology
Cambridge, Massachustts 02139

SCOPE

In many practical crystallizers the nucleation rate is dominated by interaction of crystals with their environment, that is, by secondary nucleation processes. Secondary nucleation is poorly understood and heavy reliance has been placed on empirical correlations of nucleation kinetics. Without a fundamental understanding of the processes governing secondary nucleation, the form of the function that can best correlate experimental results cannot be well established. Hence there is no sound basis for extrapolating results from one set of experimental conditions to others. As examples of the wide choice of functions available to correlate secondary nucleation, simplistic models based on the assumptions that secondary nucleation is proportional to the number of crystals, crystal perimeter, area, or mass would suggest that the nucleation rate should be proportional to the zeroth, first, second, or third moment of the crystal size distribution, that is,

$$\dot{N} = a_n \mu_n$$

where $\dot{N}$ is the nucleation rate and μ_n the nth moment of the crystal size distribution. Other models of crystallization involve collision of crystals with each other, in which case the nucleation rates would be expected to be proportional to the square of the moments of the particle size distribution. Little can be said about which moments should be used without a statement of mechanism. Additional motivation for developing mechanistic models of secondary nucleation is provided by the need to determine the dependence of nucleation rate on design parameters such as agitation rate, scale of equipment, etc.

In a previous paper (Evans et al., 1974), it has been shown that the factors influencing crystal surface morphology can be separated from those influencing collisions. In this paper, following leads provided by Clontz and McCabe (1971) and Ottens and co-workers (1972, 1973), this concept is extended. Expressions are derived for the kinetics of secondary nucleation under the assumption that the rate of nucleation is proportional to collision frequency and collision energy for each of four idealized collision mechanisms. These include (1) collision of crystals with an impeller as the crystals are swept by the impeller in steady flow, (2) collision between crystals in a turbulent flow field and various surfaces in the crystallization, (3) collision between crystals as a consequence of differences in their terminal velocities, (4) collision between crystals driven by turbulent eddy motion. The results of the analysis are found to describe adequately the kinetics of the secondary nucleation of ice. The theory provides a basis for extracting from limited experimental data generalized expressions for the kinetics of secondary nucleation useful for the design of continuous crystallizers.

CONCLUSIONS AND SIGNIFICANCE

Consideration of idealized models has identified four terms that can contribute significantly to secondary nucleation, at least for the crystallization of ice in a mechanically driven continuous crystallizer: (1) The contribution to the nucleation rate by crystals colliding with an impeller is proportional to the power input, the square root of the impeller diameter, and the 2.5th power of the mean crystal size. (2) The contribution of crystals driven into collisions with surfaces by turbulent motion is proportional to the power input, and the 3rd power of the mean crystal size. (3) The contribution by collisions between crystals whose relative motion is governed by gravitational forces is proportional to the mass concentration of crystals and the mean crystal size raised to the 5.42 power. (4) The contribution by collision between crystals driven together by turbulent eddies is proportional to the power input, the mass concentration of the crystals, and the mean crystal size raised to the 3rd power.

The models have been tested against the experimental results of Evans et al. (1974). The experimental results for ice at low concentrations could be correlated equally well by either of the first two terms and the effect on

Correspondence concerning this paper should be addressed to A. F. Sarofim. T. W. Evans is with The Upjohn Company, Kalamazoo, Michigan. G. Margolis is with Westreco, Inc., Marysville, Ohio.

the nucleation rate of adding polyethylene beads of different size could be best correlated by functional relations similar to 3 and 4 but with a dependence on mean crystal size and power input intermediate to those presented by the two limiting physical models. Judged by their success in correlating ice nucleation data, these idealized mechanistic models provide a major advance in placing the correlations of secondary nucleation on a rational basis. The models provide a means of extrapolating experimental results to conditions where shifts in the relative contributions of the different mechanisms could have a profound influence on the nucleation rate predicted.

Rates of secondary nucleation are complex and poorly understood functions of the processes that govern both crystal growth and the forces that cause the shedding of nuclei. Recent developments that have facilitated a partial modeling of the kinetics of secondary nucleation in agitated crystallizers include the demonstration that the processes of growth and removal of nuclei can be uncoupled, at least for the nucleation of ice crystals (Evans et al., 1974), the establishment that the number of secondary nuclei produced on the impact of a crystal is proportional to the impact energy (Clontz and McCabe, 1971), and the correlation of impact energy in an agitated crystallizer with design and operating variables (Ottens and co-workers, 1972, 1973). These developments are exploited in this paper in order to generate quantitative models of those components of secondary nucleation that are attributable to crystal collisions. The secondary nucleation rates predicted by the models are tested by comparisons with nucleation data on ice for which the separate contributions of crystal-surface and crystal-crystal collisions were identified by the judicious variation of surface coating and crystal concentration (Evans et al., 1974).

It is necessary to first define the forces that are responsible for secondary nucleation. Based on the results of Clontz and McCabe (1971) it will be assumed that the number of nuclei per collision is proportional to collision energy. It is recognized that Clontz's experiments do not completely define collision energy to be the driving force for secondary nucleation. For example, it has not been established whether the rate at which the energy is imparted to a crystal, by a large force of short duration or a smaller force of longer duration, influences the number of nuclei shed. The methodology developed in this paper can, however, readily admit different driving forces if new experimental or theoretical evidence suggests that this is warranted.

The rate of nucleation is then proportional to the rate of energy transfer to crystals by collision ($\dot{E}_t$), which is equal to the product of collision energy $E(r)$ and frequency of collision $\omega(r)$ of crystals in the size range r to $r + dr$ integrated over the particle size distribution, or

$$\dot{E}_t = \int_0^\infty \omega(r)\ E(r)\ f(r)\ dr \qquad (1)$$

The number of crystals S generated per unit collision energy is governed by the surface morphology and is expected to be a function of the parameters which control surface growth, including, in the case of ice: subcooling ΔT, salt concentration c, and, to a lesser extent, crystal size r, and agitation power P/V_c. The nucleation rate is then given by

$$\dot{N} = S(\Delta T,\ c,\ P/V_c,\ r,\ \ldots)\dot{E}_t \qquad (2)$$

or

$$\dot{N} = S(\Delta T,\ c,\ P/V_c,\ r,\ \ldots) \int_0^\infty \omega(r)\ E(r)\ f(r)dr \qquad (3)$$

Although the value of S must be established empirically, the uncoupling of the processes governing the growth of potential nuclei from the removal processes provides a means of quantitatively taking into account the effect of changes in design and operation that influence E_t. It should be noted that S accounts for all the effects of subcooling and salt concentration on secondary nucleation, neglecting second-order effects due to changes in physical properties which may influence E_t. It will also be shown that $\dot{E}_t$ accounts for most of the effects of crystal size and agitation power on secondary nucleation, thus permitting the conclusions derived on the effects of these variables for one salt solution to be applied to another. The emphasis in the subsequent sections will be on the calculation of $\dot{E}_t$.

CRYSTAL-CRYSTALLIZER COLLISIONS

The relative motion between crystals and surfaces necessary for collision is attributable either to the action of turbulent eddies or to the large-scale circulation induced by the impeller. Although the two factors act together, they will be considered separately in order to simplify the analysis. Collisions driven by the circulation in a crystallizer are mainly with the impeller (Evans et al., 1974) and the analysis will therefore be further simplified by focusing on this source of secondary nucleation. The method of analysis, however, is general and may be applied to the prediction of secondary nucleation contributed by crystal collisions with baffles and with impellers of configuration other than that treated here.

Collisions Driven by Bulk Motion

The value of $\dot{E}_t$ contributed by collisions of crystals with the impeller will be proportional to collision frequency, dependent on circulation time (V_c/Q) and efficiency of collection (η_p), and kinetic energy at impact. The efficiency of collection and collision energy were obtained by the numerical simulation of the trajectory of the particles past the segments of the impeller. Several simplifications were introduced (1) blade element theory (O'Brien, 1962) was used to approximate the three-dimensional flow near the impeller by two-dimensional flow past the blade elements with allowance for variation in velocity with distance from the axis, (2) the potential flow solution for the flow past the blade elements was utilized in most of the calculations; for a few cases allowance was made for a boundary layer, (3) the particle trajectories were calculated using different approximations, first assuming the particles followed the streamlines, then including allowance for the viscous forces, pressure area forces, and the Basset forces (Hinze, 1959), (4) the approach of a particle to within a particle radius of the blade element was counted as a collision. The detailed development of this model follows. Equation (1) may be rewritten as

$$\dot{E}_t = \frac{Q}{2V_c} \int_0^\infty \eta_p(r)\ m(r)\ v_c^2(r)\ f(r)\ dr \qquad (4)$$

Utilization of $Q = kN(2R_a)^3$, where $k = 0.15\pi p$ (Brothman et al., 1943) for the volumetric discharge rate of the marine propellor and blade element theory to approximate the flow past the impeller as that of a steady flow of fluid approaching an impeller element at a normalized radius

R' with a velocity v_∞ and at an angle α (see Figure 1), yields

$$\dot{E}_t = 0.478 n_b \left(\frac{\rho_i}{\rho_f}\right)\left(\frac{W}{R_a}\right)\left(\frac{k}{N_{p0}}\right)\left(\frac{P}{V_c}\right)\int_0^\infty r^3 f(r) \int_0^1 h(R', p) \quad (5)$$

$$\eta(r, W, v_\infty, \alpha)\ \epsilon(r, W, v_\infty, \alpha)\ dR'\ dr$$

where

$$h(R', p) = \frac{\sin^3\alpha}{\sin(\theta - \alpha)}\left((\pi R')^2 + (.6p)^2\right)$$

η is the collection efficiency of the blade element, which is defined in terms of the line segment (ab). ϵ is the square of the collision velocity normalized by $v_\infty \sin\alpha$ (the velocity of the fluid normal to the blade at long distances from the blade).

Outside of the innermost integral, the form of Equation (5) is identical to that derived by Ottens et al. (1972) by qualitative reasoning. The important difference in Equation (5) to that derived by Ottens is that this model yields a quantitative value for $\dot{E}_t$ which can be compared with other mechanisms for collision. Also the innermost integral slightly affects the functional form of the equation for $\dot{E}_t$.

The numerical solution for η and ϵ for a marine propellor with a pitch of 1.5 (simulating the experiments by Evans, 1973) could be correlated by

$$\eta = (r/W)^{1/2}$$
$$\epsilon = 0.06\ (W/r) \quad (6)$$

It was assumed in determining these equations that the particles follow the streamlines. This is valid for particle parameters $(\rho_f r^2 V_\infty / W\mu)$ less than 0.1, which is usually true for cases of interest here. Evans (1973) studied the particle dynamics for higher values of the particle parameter. Surprisingly, the product of η and ϵ increases with increasing W or decreasing r. An explanation for this unexpected result is that the collisions which make the greatest contribution to ϵ occur at the tips of the blade element, at locations where the fluid is accelerating to round the tip and where crystals closest to the blade (small r/W) have the greatest velocity toward it. Allowance for a boundary layer and the pressure gradient forcing the lighter ice crystals away from the agitator blades had negligible effect on the product $\eta\epsilon$.

Substitution of Equation (6) into Equation (5) yields

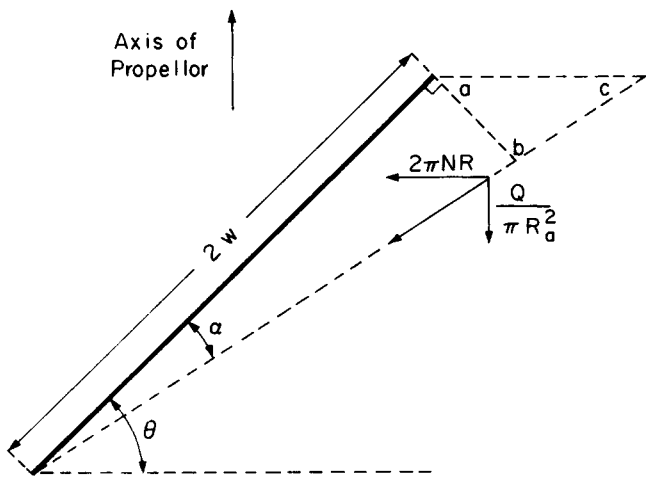

Fig. 1. Blade element.

$$\dot{E}_t = 0.0043\left(\frac{\rho_i}{\rho_f}\right)\left(\frac{k}{N_{p0}}\right)\left(\frac{P}{V_c}\right)(R_a)^{1/2}\,\mu_{2.5} \quad (7)$$

The constants and exponents in Equation (7) are quantitatively applicable only to the case in question, but they can be readily derived for impellers of different configuration and particles whose dynamics may differ from those of ice.

Collisions Driven by Turbulence

Considering the contribution to $\dot{E}_t$ by the collisions with the agitator and baffles of crystals following small-scale turbulent motion in their vicinity, it is assumed that:

1. The crystals follow any turbulent eddy of size greater than themselves, but are uninfluenced by smaller eddies
2. The number of crystals per unit volume is uniform through the crystallizer.

Consider a particle a distance ρ from a surface (see Figure 2). Turbulent eddies with a characteristic scale greater than that of the particle are assumed to transport the particle with a velocity equal to the velocity of the eddy, over a distance (on the average) equal to the scale R. The rate of energy transferred to crystals by this mechanism can be approximated by

$$\dot{E}_t = \int_0^\infty \int_r^{R_m + r} \int_{\max(\rho - r, r)}^{R_m} [Pr(\rho)\ \omega(\rho, r, R)] \left[\frac{1}{2} m(r)\ \epsilon_t(R)\right] f(r)\ dR\ d\rho\ dr \quad (8)$$

The innermost integral is over all eddy sizes which influence the crystal and may induce a collision with the obstacle. The next integration is over the volume within which the crystal may lie. R_m is the maximum eddy size which is turbulent relative to the obstacle; for a marine propellor it can be approximated by

$$R_m = W \sin\alpha$$

Crystals may travel in any direction depicted by the sphere in Figure 2, but only those which travel within a solid angle ϕ_c will collide. The collision frequency is inversely proportional to the time required for the crystal to traverse the distance to the obstacle. The collision velocity is taken to be the component of velocity resolved normal to the obstacle at impact. The mean square velocity of eddies in the size range R to $R + dR$ can be equated to $\overline{E}(R)dR$, where $\overline{E}(R)$ is the turbulent energy spectrum approximated, within the universal equilibrium range (Hinze, 1959),

$$E(R) = a(P/M)^{2/3}\ (R)^{-1/3} \quad (9)$$

By applying the above arguments, Equation (8) may

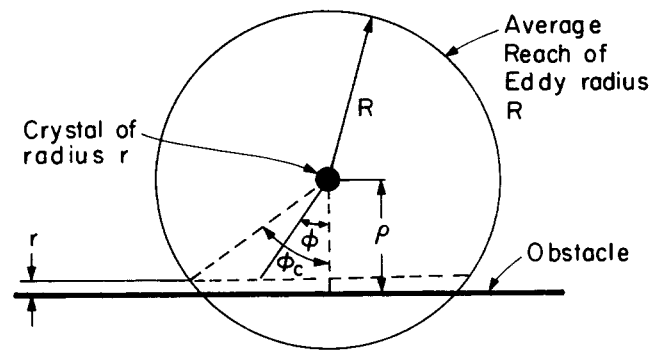

Fig. 2. Schematic of crystal-crystallizer collisions driven by turbulence.

be rewritten as

$$\dot{E}_t = 0.97\, a^{2/3} \left(\frac{\rho_i}{\rho_f}\right)\left(\frac{P}{V_c}\right)\left(\frac{A}{V_c}\right)\mu_3\, R_m \quad (10)$$

Comparison with Experimental Results

Two types of the experimental results presented by Evans (1973) can be used to test the models. The first is n, which is a measure of the dependence of the nucleation rate on crystal size. From the experimental results it was concluded that n was between 2 and 5 with the value of 3 being most probable. The other experimental result sensitive to mechanism is the dependency of the nucleation rate on the agitation power or the rotational speed of the agitator. The nucleation rate for ice (Brian et al., 1974) is found to depend on P/V_c to the 0.95 power for agitation powers greater than 560 J/m^{3}s, if it is accepted that n equals 3, and if the growth rate is taken to be proportional to $(P/V_c)^{0.15}$ (Brian et al., 1969). For collisions driven by bulk motion [see Equation (7)], the nucleation rate is predicted to be dependent on the 2.5th power of the crystal radius ($n = 2.5$) and the first power of P/V_c. For collisions driven by the turbulent motion, Equation (10) reveals that the nucleation rate is dependent on the first power of P/V_c and n equals 3.

Both models predict the experimental results equally well, and reinforce the statement made earlier that the dependence of S on r and P/V_c is small. The small difference between the functional form of the two mechanisms for secondary nucleation (bulk and turbulent motion) is not surprising since the major factor determining the dependency of the nucleation rate on the crystal size and the agitation power is the assumption that the physical driving force of removal is the collision energy, Equation (2). Thus, the above agreement between theory and experiment does not distinguish between the fluid mechanical driving forces but verifies that the collision energy is the driving force for the removal of nuclei.

It is possible, however, to determine which is the dominant mechanism producing collisions by comparing the calculated rate of total collision energy for the two models. For crystallizers which are geometrically similar to the experimental, the ratio of the total rates of collision energy for collisions driven by the bulk flow to those driven by turbulence is presented in Table 1 for various ratios of the propellor radius (R_a) to the average crystal radius ($\bar{r}$).

It was assumed in applying the turbulence model that the turbulent intensity was uniform throughout the crystallizer. In practice, the turbulent intensity in the region near the agitator may be greater than that in the bulk by factors of ten or more (Wadia, 1974). Thus, the ratios presented in Table 1 are possibly a factor of 10 or more too large. The ratios ($R_a/\bar{r}$) for the experimental system are in the range 10^2 to 10^3, and thus it is not possible to determine at this stage which driving force makes the major contribution to the nucleation rate.

Table 1. Comparison of Models for Crystal-Crystallizer Collisions

$\frac{R_a}{\bar{r}}$	$\frac{\dot{E}_t\ (\text{Bulk flow})}{\dot{E}_t\ (\text{Turbulence})}$
10^2	2.2
10^3	7.0
10^4	22
10^5	70

CRYSTAL-CRYSTAL COLLISIONS

Two models were developed to characterize the collisions of the crystals with each other. The first visualizes the crystals colliding as a result of the dependency of the terminal velocity due to gravity on the crystal size. As a consequence of their greater terminal velocity, the larger particles collide with the smaller crystals. The second model visualizes particle collisions driven by the turbulence within the agitated crystallizer. As before, it is assumed that crystals will follow any eddy of size greater than themselves but will not follow an eddy of lesser size. Thus, smaller crystals will follow a greater range of eddy sizes and collide with larger crystals. A corollary of the basic hypothesis is that the crystals will have motion relative to each other and collide only if the crystals are of different size.

Although the driving forces for these two models are different, the basic treatment is identical and therefore they will be developed here simultaneously. The starting point for this development is a modified form of the basic equation for $\dot{E}_t$ [Equation (1)]

$$\dot{E}_t = \frac{1}{2}\int_0^\infty \int_0^\infty q(r_1, r_2)\, E(r_1, r_2)\, f(r_1)\, f(r_2)\, dr_1\, dr_2 \quad (11)$$

where $q(r_1, r_2)\, f(r_1)\, f(r_2)\, dr_1\, dr_2$ is the collision frequency per unit volume between crystals of size r_1 to $r_1 + dr_1$ and r_2 to $r_2 + dr_2$, and $q(r_1, r_2)$ is the volume containing crystals of size r_2 with which a crystal of size r_1 collides in a unit time

$$q(r_1, r_2) = \pi(r_1 + r_2)^2\, v(r_1, r_2)$$

The collision energy is the maximum kinetic energy which is converted to deformation energy during impact:

$$E(r_1, r_2) = \frac{1}{2}\left(\frac{m(r_1)\, m(r_2)}{m(r_1) + m(r_2)}\right) v^2(r_1, r_2)$$

For the case of collisions driven by gravity, it is assumed that the crystals travel at their terminal velocities. For most cases of practical interest, the Reynolds number of the crystal is in the regime where the drag coefficient is inversely proportional to the 0.6 power of the Reynolds number. Thus, the relative velocity can be expressed as

$$v(r_1, r_2) = 0.3\left[\frac{(\rho_f - \rho_i)g}{\rho_f}\left(\frac{\rho_f}{\mu}\right)^{0.6}\right]^{0.715} |r_1^{1.14} - r_2^{1.14}|$$

Again the turbulent energy spectrum in the universal equilibrium range can be represented by Equation (9). $\bar{E}(R)dR$ is the mean square of the velocities of all eddies between the sizes R and $R + dR$; therefore, the mean square of the velocities of all eddies between the sizes r_1 and r_2 can be expressed by

$$v^2(r_1, r_2) = \frac{2}{3}\int_{r_1}^{r_2} \bar{E}(R)\, dR = a(P/M)^{2/3} |r_1^{2/3} - r_2^{2/3}|$$

The component of $\dot{E}_t$ contributed by collision between crystals driven by gravity is obtained by substituting the above relationship into Equation (11). The result is

$$\dot{E}_t = K_g\, f^2(0)\, \bar{r}^{\,10.42} \int_0^\infty T_g(r_2')\, \exp(-r_2')\, dr_2' \quad (12)$$

where

$$K_g = 0.09\, \rho_i \left[\frac{(\rho_f - \rho_i)g}{\rho_f}\left(\frac{\rho_f}{\mu}\right)^{0.6}\right]^{2.15}$$

$$T_g(r_2') = \int_0^\infty t_g(r_1', r_2')\, \exp(-r_1')\, dr_1'$$

$$t_g(r_1', r_2') = (|r_1'^{1.14} - r_2'^{1.14}|)^3\, (r_1' + r_2')^2\, \frac{r_1'^3\, r_2'^3}{r_1'^3 + r_2'^3}$$

Similarly the component of $\dot{E}_t$ contributed by collisions driven by the turbulence is given by

$$\dot{E}_t = K_t\,(P/V_c)\,f^2(0)\,\bar{r}^8 \int_0^\infty T_t(r_2')\exp(-r_2')\,dr_2' \tag{13}$$

where

$$K_t = 3.3\,a^{3/2}\left(\frac{\rho_l}{\rho_f}\right)$$

$$T_t(r_2') = \int_0^\infty t_t(r_1', r_2')\exp(-r_1')\,dr_1'$$

$$t_t(r_1', r_2') = \left(\left|r_1'^{2/3} - r_2'^{2/3}\right|\right)^{3/2}(r_1' + r_2')^2\,\frac{r_1'^3\,r_2'^3}{r_1'^3 + r_2'^3}$$

The above equations were derived for a continuous MSMPR crystallizer in which the particle size distribution is given by $f(0)\exp(-r')$, as would be expected when nuclei are born at near zero size and the growth rate is independent of particle size. It should be noted that t_g, t_t, T_g and T_t are dimensionless functions independent of any design variable or physical parameter of the crystallizing system.

In Figure 3 $t_g\exp(-r_1')$ normalized by the maximum value of this function is plotted against r_1' for various values of r_2'. Similarly $T_g\exp(-r_2')$ normalized by the maximum value of this function is plotted against r_2' in Figure 4. The corresponding plots for the case in which turbulent eddies drive the collisions are shown given in Figures 5 and 6.

The functions $t_g\exp(-r_1')$ and $t_t\exp(-r_1')$ are most readily visualized in terms of an experimental situation in which particles of a single size r_2' are added to the crystallizer in concentrations large relative to the concentration of crystals of all other sizes. For this situation, $t_g\exp(-r_1')$ and $t_t\exp(-r_1')$ represent the contribution to the overall nucleation rate of crystals of size r_1' colliding with the added particles. It may be seen from Figure 3 that when

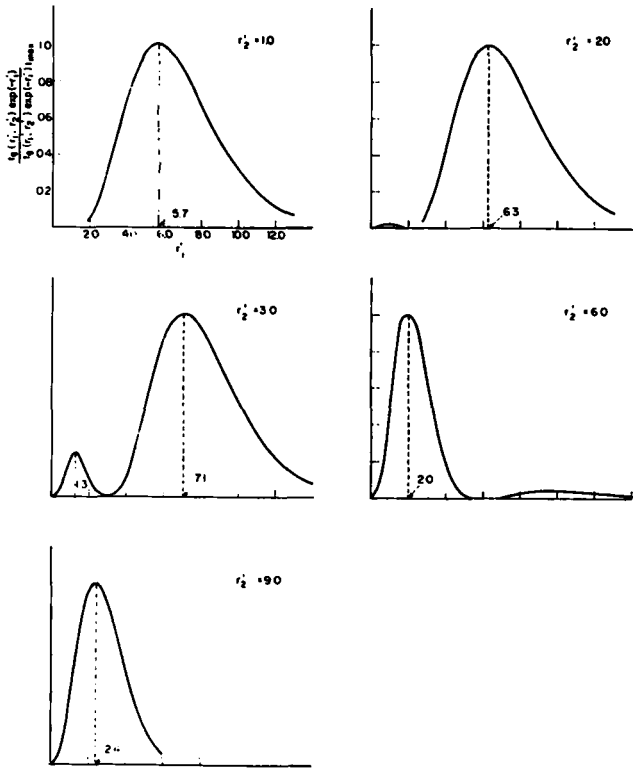

Fig. 3. Normalized $t_g\exp(-r_1')$ vs. r_1' for various r_2'.

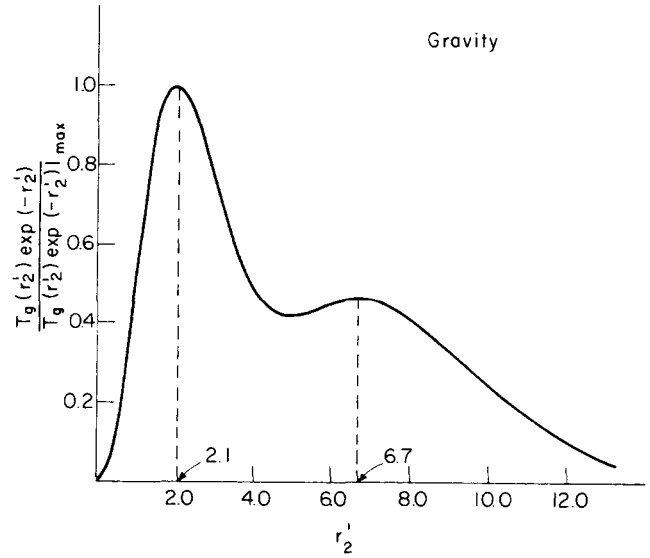

Fig. 4. Normalized $T_g\exp(-r_2')$ vs. r_2'.

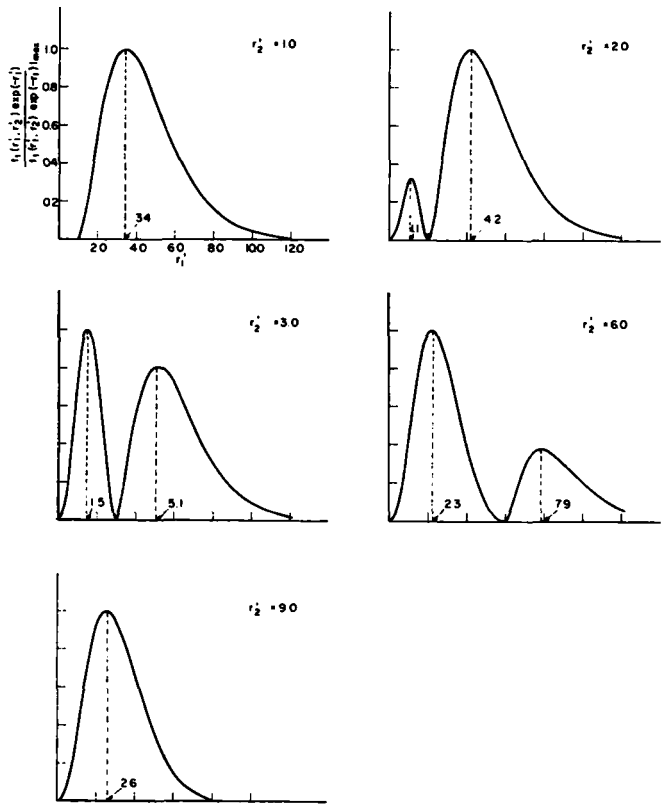

Fig. 5. Normalized $t_t\exp(-r_1')$ vs. r_1' for various r_2'.

the size of added particles is equal to the mean size of the other crystals, practically all the nucleation is due to collisions of the added particles with crystals of larger size. As the size of the added particles is increased to $2\bar{r}$, the collisions of the added particles with smaller crystals makes a noticeable but small contribution to the overall nucleation rate. This contribution is further increased by increasing the size of the added particles to $3\bar{r}$. When the size is increased to $6\bar{r}$, the major contribution to the overall nucleation rate is the collisions with the smaller crystals, while collisions with the larger crystals make a minor contribution. Finally for r_2' equal or greater than $9\bar{r}$, secondary

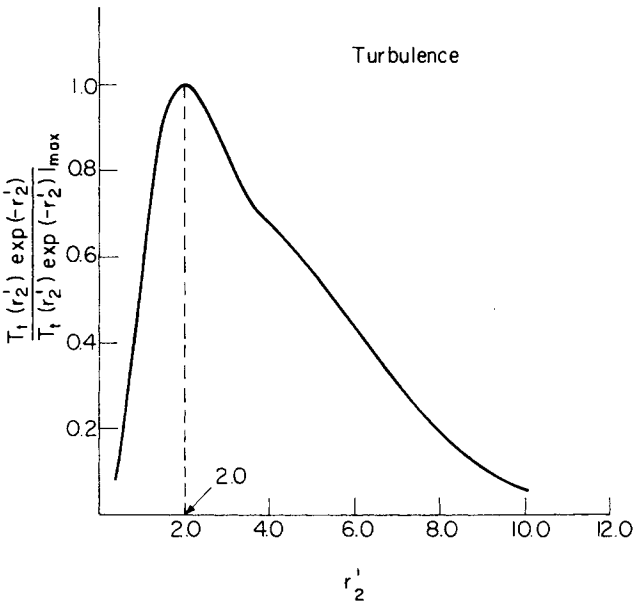

Fig. 6. Normalized $T_t \exp(-r_2')$ vs. r_2'.

TABLE 2. COMPARISONS OF EXPERIMENTAL RESULTS WITH PREDICTIONS OF NUCLEATION MODELS FOR CRYSTAL-CRYSTAL COLLISIONS

Value compared	Experiment	Gravity-driven collisions	Turbulence-driven collisions
n in $\dot{N} \propto \mu_n$ f(added particles)	2	1.8	2.1
c in $\dot{N} \propto (P/V)^c$	0.6	0	1.0
s in $\dot{N} \propto (\bar{d}$ added particles$)^s$	5	6	4
$\dfrac{(\dot{N}$ expt simulating cont MSMPR cryst$)}{(\dot{N}$ predict cont MSMPR cryst from $\dot{N}$ expt for $\bar{d} = 0.3$ mm$)}$	—	0.71	1.37
$\dfrac{(\dot{N}$ expt simulating cont MSMPR cryst$)}{(\dot{N}$ predict cont MSMPR cryst from $\dot{N}$ expt for $\bar{d} = 0.9$ mm$)}$	—	0.87	0.37

nucleation is due principally to collisions between the added particles and smaller crystals. A similar phenomenon is observed in Figure 5 for collisions driven by turbulence. However, the shift with increasing r_2' in the importance of the collisions of added particles with larger crystals to those with smaller crystals is more gradual.

A comparison of the figures for the two collision driving forces shows that the two peaks are always closer together for collisions driven by turbulence (that is best observed in the two plots for r_2' equals 3), a consequence of the greater dependency of $v(r_1, r_2)$ on the difference between r_1 and r_2 for gravity driven than turbulence driven collisions.

The functions $T_g \exp(-r_2')$ and $T_t \exp(-r_2')$ represent the nucleation due to the collisions of the crystals of radius r_2' with all other crystals in a continuous MSMPR crystallizer. $T_g \exp(-r_2')$ exhibits two peaks since major weight is given to collisions between crystals of widely differing size, that is, that of the smaller crystals with the larger crystals. $T_t \exp(-r_2')$ has but one peak with a slight inflection point.

Comparison with Experimental Results

Four types of experimental results presented by Evans et al. (1974) can be used to test the nucleation models. The first is n or the experimentally measured dependency of the actual nucleation rate on the crystal size. From the experimental results it was concluded that n was between 1 and 3 with the value of 2 being most probable. The second is the dependency of the nucleation rate on the agitation power. The dependence of nucleation rate on agitation power is inferred to be to the 0.6 power for an n of 2 and a dependence of crystal growth rate on the 0.15 power of P/V_c.

The remaining experiments deal with the dependency of the nucleation rate on the size of the added particles. Comparison of the nucleation rates with added particles with diameters of 0.3 and 0.9 mm showed a dependence of the nucleation rate on the fifth moment of the added particle size over this range. Nucleation rates were also measured with the addition of particles having a size distribution matching that expected in a continuous MSMPR crystallizer. Given the nucleation rate data for added particles with diameters of 0.9 or 0.3 mm, it is possible to exploit the models to predict the nucleation rate for a distribution of particles simulating continuous MSMPR crystallizer operation. The experimental results are compared with the theoretical predictions in Table 2.

The theories are in basic agreement with the experimental results. The comparisons which are most sensitive to the physical driving force which induces the collisions are the last four in Table 2. For all of these comparisons except the last, the experimental results are intermediate to those predicted by the two driving forces.

In assessing the validity of the last three comparisons, consider Figures 3 and 5. These graphs represent the relative contribution of crystals of radius r_1' colliding with added particles of radius r_2' to the overall nucleation rate. In the complementary experimental program (Evans, 1973), the maximum size within the crystallizer in which the nucleation rate was measured was approximately $6\bar{r}$. For $r_2 = 9\bar{r}$ (approximate case for $\bar{d} = 0.9$ mm), the collisions of the added particles with the crystals larger than $6\bar{r}$ make a negligible contribution to the nucleation rate. While, for $r_2 = 3\bar{r}$, collisions of the added particles with crystals larger than $6\bar{r}$ make a major contribution to the nucleation rate. Thus, when making the third comparison in Table 2, it was essential to correct for a finite maximum crystal size. Unfortunately, since a batch crystallizer was employed experimentally, the maximum crystal varies with time. The calculation presented in Table 2 was crudely corrected by assuming a constant maximum crystal size of $6\bar{r}$. A similar correction was made for the last two calculations.

By comparing the total rate of collision energy predicted for each of these models, it would also be possible to discern which driving force dominates. Two comparisons will be performed here. First, a comparison will be made for the experimental case where particles of a single size were added to the crystallizer. The ratios of $\dot{E}_t$ for the turbulence model to that for the gravity model are presented in Table 3. Typical values of $\bar{r}$ are in the range of 0.05 to 0.10 mm and $\bar{d}'/2$ in the range of 6.0 to 9.0. For these values the rate of total collision energy predicted by the turbulence model is approximately two orders of magnitude greater than those predicted by the gravity model.

For an agitation power of 1000 J/m^{3}s and ice, the ratio

Table 3. Relative Contribution of Turbulence and Gravity Models for Experimental System
$P/V_c = 1000$ J/m³s

$\bar{d}'/2\ \bar{r}$(mm)	0.033	0.05	0.075	0.10
1.0	2080	770	287	138
3.0	2050	755	280	135
6.0	1810	660	245	128
9.0	618	223	85	48

Table 4. Relative Contributions of Turbulence and Gravity for a Continuous MSMPR Crystallizer
$P/V_c = 1000$ J/m³s

$\bar{r}$(mm)	Ratio
0.033	1,640
0.10	111
0.33	6.25
1.00	0.42

of $\dot{E}_t$ for turbulence driven collisions to that for gravity driven collisions in a continuous MSMPR crystallizer is presented in Table 4. The conclusion to be drawn from this table is that, as the average crystal size is increased, the collisions driven by gravity become more important relative to those driven by turbulence. This can be explained by the greater dependence of collision velocity on the difference between the sizes of two crystals for the gravity-driven collisions. As the average crystal size increases, the crystal size distribution becomes broader and the gravity-driven terms more important.

COMPARISON OF THE MECHANISMS

Theory versus Experiment

The contributions of crystal-crystallizer and crystal-crystal collisions to the overall nucleation rate for an agitation power of 1000 J/m³s and 10% weight ice were presented by Evans et al. (1974). The experimental ratio of the rates for these two mechanisms was 2.5. Since $\dot{E}_t$ for crystal-crystallizer collisions is greater for collisions driven by the bulk motion and $\dot{E}_t$ for crystal-crystal collisions is greater for collisions driven by turbulence, the resulting rates for these driving forces will be employed to determine a theoretical ratio of the mechanisms. The calculated ratio is 2.2. The agreement between theory and experiment is surprisingly good. This comparison is very sensitive to the physical driving force of the relevant collisions, and thus this agreement gives credence to the driving forces chosen to model these removal mechanisms.

Design Equation

The models presented in this paper can be summarized by the following four-term design equation

$$\beta = \frac{\dot{N}}{\mu_0} = \left[K_b \left(\frac{P}{V_c}\right)\left(\frac{k}{N_{p0}}\right) R_a^{1/2}\, \bar{r}^{2.5} + K_{ct}\left(\frac{P}{V_c}\right)\bar{r}^3 + K_g x\, \bar{r}^{5.42} + K_t \left(\frac{P}{V_c}\right) x\, \bar{r}^3 \right] S(\Delta T, c) \tag{14}$$

where the first term on the right is the nucleation due to crystals colliding with the crystallizer driven by the bulk flow, the second term is collisions with the crystallizer driven by turbulence. The third and fourth terms represent crystal-crystal collisions driven by gravity and turbulence, respectively.

In this design equation, the two terms for crystal-crystallizer collisions are dependent on P/V_c to the first power. While for collisions of the crystals with one another, the rate constant is dependent on the first power for collisions driven by turbulence but is independent of P/V_c for collisions driven by gravity. Thus, one would expect that the relative importance of crystal-crystal collisions driven by gravity will decrease with increasing agitation power.

In a continuous MSMPR ice crystallizer, average crystal size increases with increased residence time. For crystal-crystallizer collisions, the power dependencies on the average crystal size are 2.5 and 3.0, respectively, for the collision driving forces of bulk flow and turbulence. While, for crystal-crystal collisions the power dependencies are 3.0 for turbulence and 5.42 for gravity. Thus, it is expected that as the average residence time is increased, crystal-crystal collisions driven by gravity will become more important relative to the other mechanisms and collision driving forces.

All terms for the collision and removal driving forces are independent of the size of the crystallizer except for crystal-crystallizer collisions driven by the bulk motion. Since this term is dependent on the radius of the agitator to the half power, this removal and collision driving force should become more dominant with increasing equipment scale.

Finally, for systems crystallizing other chemicals, crystal-crystal collisions driven by gravity are most sensitive to the density difference between the liquid and solid phases. Thus, it is expected that this removal mechanism and collision driving force will be more important in systems for which the difference in specific gravity between liquid and solid is large.

NOTATION

a = constant equals 1.436 (Grant et al., 1962)
A = area of obstacle
c = salt concentration, Kg(salt)/Kg(total)
$\bar{d}$ = diameter of added particles
$\bar{d}'$ = $\bar{d}/\bar{r}$
E = collision energy, J/collision
$\dot{E}_t$ = total rate of collision energy, J/m³s
$\bar{E}$ = turbulent energy spectrum, m/s²
f = crystal frequency distribution, crystals/m⁴
g = acceleration due to gravity
h = function, defined after Equation (5)
k = discharge coefficient of the agitator
m = mass of crystal
M = total mass within the crystallizer
n = power dependency of the actual nucleation rate on the crystal radius
n_b = number of blades per propellor
N = rotational speed of the agitator, cycles/s
$\dot{N}$ = actual nucleation rate, nuclei/s m³
N_{p0} = power number of the agitator
p = pitch of marine propellor
P = agitation power, J/s
$Pr(\rho)$ = probability of a crystal being a distance ρ from obstacle
$q(r_1, r_2)$ = volume containing crystals of size r_2 with which a crystal of size r_1 collides in a unit time, collision · m³/s(crystals)²
Q = volumetric discharge rate of agitator
r = characteristic dimension of crystal, crystal radius
$\bar{r}$ = average crystal size, m
r_1, r_2 = crystal radii for models of crystal-crystal collisions

$r_1', r_2' = r_1/\bar{r}, r_2/\bar{r}$
R = propellor radial coordinate or radius of turbulent eddy
R' = R/R_a
R_a = radius of propellor
R_m = maximum eddy size which is turbulent relative to obstacle
S = characterizes crystal surface morphology, nuclei/unit driving force
t_g, T_g = functions defined after Equation (12)
t_t, T_t = functions defined after Equation (13)
ΔT = solution subcooling
$v(r_1, r_2)$ = velocity of crystal radius r_1 relative to crystal radius r_2
v_c = collision velocity
v_s = velocity of fluid relative to blade element
V_c = volume of crystallizer
W = half width of blade element
x = weight fraction of crystals, Kg(crystal)/Kg(total)

Greek Letters

α = hydrodynamic angle
β = nucleation rate per crystal, nuclei/crystal · s · m^3
ϵ = square of collision velocity normalized with respect to $v_s \sin\alpha$
ϵ_t = square of collision velocity, m/s^2
η = collection efficiency of blade element
η_p = collection efficiency of propellor
θ = angle of propellor blade relative to the plane of the propellor
μ = dynamic viscosity
$\mu_n = \int_0^\infty r^n f(r)\, dr$
ρ = distance of crystal from obstacle
ρ_f = density of fluid
ρ_i = density of crystal
ϕ = solid angle for crystal colliding with obstacle
ϕ_c = maximum solid angle
ω = collision frequency, collision/crystal · s

Subscripts

b = crystal-crystallizer collisions driven by the bulk flow
ct = crystal-crystallizer collisions driven by turbulence
g = crystal-crystal collisions driven by gravity
t = crystal-crystal collisions driven by turbulence

LITERATURE CITED

Brian, P. L. T., H. B. Hales and T. K. Sherwood, "Transport of Heat and Mass Between Liquids and Spherical Particles in an Agitated Tank," *AIChE J.*, **15**, 727 (1969).

Brian, P. L. T., A. F. Sarofim, T. W. Evans, and S. G. Kane, "The Kinetics of the Secondary Nucleation of Ice: Implications to the Operation of Continuous Crystallizers", submitted to *Desalination* (1974).

Brothman, A., A. P. Weber, and E. Z. Barish, *Chem. Metal. Eng.*, **50**, 107 (1943).

Clontz, N. A., and W. L. McCabe, "Contact Nucleation of Magnesium Sulfate Heptahydrate," *Chem. Eng. Progr. Symp. Ser. No. 110*, **67**, 6 (1971).

Evans, T. W., "Mechanisms of Secondary Nucleation during the Crystallization of Ice," Ph.D. thesis, M.I.T., Cambridge, Mass. (1973).

———., G. Margolis, and A. F. Sarofim, "Mechanisms of Secondary Nucleation in Agitated Crystallizers," *AIChE J.*, **20**, (1974).

Grant, H. L., R. W. Stewart, and A. Moilliet, "Turbulence Spectra from a Tidal Channel," *J. Fluid Mech.*, **12**, (2), 241 (1962).

Hinze, J. O., *Turbulence*, McGraw-Hill, New York (1959).

O'Brien, T. P., *The Design of Marine Screw Propellors*, Hutchinson & Co., Ltd., London (1962).

Ottens, E. P. K., A. H. Janse, and E. J. deJong, "Secondary Nucleation in a Stirred Vessel Cooling Crystallizer," *J. Crystal Growth*, **13/14**, 500 (1972).

Ottens, E. P. K., and E. J. deJong, "A Model for Secondary Nucleation in a Stirred Vessel Cooling Crystallizer," *Ind. Eng. Chem. Fundamentals*, **12**, 179 (1973).

Wadia, P. H., "Mass Transfer from Spheres and Discs in an Agitated Tank," Sc.D. thesis M.I.T., Cambridge, Mass. (1974).

Manuscript received November 9, 1973; revision received May 24 and accepted May 30, 1974.

Experimental Investigation of Polarization Effects in Reverse Osmosis

With a Mach-Zehnder interferometer, salt concentration profiles were measured in a reverse osmosis system under natural convection with the membrane in a vertical position. The measured concentration profiles compared favorably with those predicted theoretically as long as the motion remained laminar. At large distances from the leading edge, however, the flow developed a wavy pattern, especially for bulk salt concentrations in excess of 0.1 moles/liter. As expected, whenever this motion became especially pronounced, the concentration of salt at the membrane surface was less and the production rate of fresh water greater than that predicted using the laminar analysis.

A. R. JOHNSON

Department of Chemical Engineering
Stanford University
Stanford, California 94305

SCOPE

One of the more promising techniques of desalination is the so-called "reverse osmosis" process, in which separation is accomplished by applying sufficient pressure to a salt solution to force the water through a semipermeable membrane, that is, a membrane that will preferentially allow the passage of water molecules over salt ions. The process suffers from the fact, however, that as the water

A. R. Johnson is with Kaiser Aluminum & Chemical Company, Permanente, California 95014.